UNIVERSITY OF TARTU

Institute of Chemistry

Chair of Colloid and Environmental Chemistry

Illia Shypunov

Highly active Ag-MnO_x/C catalysts for oxygen electroreduction

Master's Thesis

Supervisors:

Nadežda Kongi, PhD

Kaido Tammeveski, PhD

Tartu 2015

Table of contents

List of abbreviations

AB	Acetylene black
BE	Binding energy
CNT	Carbon nanotubes
CV	Cyclic voltammetry
DMF	Dimethylformamide
DMFC	Direct methanol fuel cell
$E_{1/2}$	Half-wave potential
EDX	Energy dispersive X-ray spectroscopy
G	Graphene
GC	Glassy carbon
GPES	General purpose electrochemical system
K-L	Koutecky-Levich
MCMB	Mesocarbon microbeads
MWCNT	Multi-wall carbon nanotubes
n	Number of electrons transferred
ORR	Oxygen reduction reaction
RDE	Rotating disk electrode
RM	Reference material
SEM	Scanning electron microscopy
SWCNT	Single-wall carbon nanotubes
XPS	X-ray photoelectron spectroscopy
XRF	X-ray fluorescence

1. Introduction

Oxygen reduction reaction (ORR) is one of the pivotal processes in electrochemistry, especially in energy conversion systems such as fuel cells. Oxygen electroreduction itself is a sluggish process. In order to accelerate the ORR kinetics to reach practical usable level in a fuel cell, an active cathode catalyst for ORR is needed [1]. Noble metals, such as Pt and Pt alloys are known to exhibit the best overall ORR performance as catalyst materials [2]. Nevertheless, their high cost, scarcity, and weak durability severely hinder their applicability to broad commercialization. Hence, the establishment of non-precious metal catalysts with comparable ORR activity to Pt-based catalysts but with higher durability, much lower cost is highly desirable in the fuel cell development [3]. Powerful research activity in the last decade yielded considerable amount of carbon-based composites as efficient elelectrocatalysts [4-6]. Among noble-metal-free alternatives, manganese oxides have received much attention because of their high element abundance, low cost, lower environmental impact, and moderate activity. Compared with noble metal catalysts, manganese oxides are generally less active, particularly in terms of overpotentials and their capability to catalyze 4-electron reduction of O_2 [7,8]. Usual strategies to improve the electrocatalytic performance of manganese oxides consist of doping with cations [9], coating with metals [10], and integrating conductive nanostructures [11]. Despite the fact that these approaches have proven effective, they are rather complicated and costly. Enhancing the activity of manganese oxides through simple and economic alternative ways is a key for investigating high-performing manganese-based electrocatalysts.

Silver is favorable noble metal catalyst. Being less expensive than Pt, silver has shown relatively high ORR activity and stability with similar loadings in alkaline electrolyte. Both materials are known to promote the ORR via direct 4-electron pathway. Silver is considered as feasible alternative to replace Pt in alkaline fuel cell cathodes [12-14].

Motivated by promising electroactivity of Ag/MnO_x supported catalysts we have established 3 different methods of electrocatalyst synthesis. Carbon nanotubes (CNT) and graphene were modified with manganese oxide and silver was attached chemically and by electrodeposition. The electrocatalytic activity and durability of the prepared catalysts toward the ORR in 0.1 M KOH solution have been studied and compared with the bulk Ag and Pt electrodes in detail.

2. Literature overview

2.1. Graphene and carbon nanotubes

Graphene is one of the most attractive carbon nanostructures of the past decade with unique mechanical, electrical, and optical properties that have been attracted tremendous interest in academics and industry. Following the isolation of graphene and mainly the establishment of several procedures for its production in sufficient quantities, several researchers – inspired from analogous successful chemical modification of fullerenes and carbon nanotubes – have performed a great number of chemical functionalization of graphene with analogous success. [15]

Graphene is an allotrope of carbon in the form of a two-dimensional, atomic-scale, hexagonal lattices in which one atom form each vertex. It is the basic structural element of other allotropes, including graphite, charcoal and carbon nanotubes. It can also be considered as an indefinitely large aromatic molecule, the limiting case of the family of flat polycyclic aromatic hydrocarbons. [16]

It is the thinnest material known to man at one atom thick, the lightest material known (with 1 square meter coming in at approximately 0.77 mg), the strongest material discovered (between 100-300 times stronger than steel and with a tensile stiffness of 150,000,000 psi), the best conductor of heat at room temperature (at $(4.84\pm0.44) \times 10^3$ to $(5.30\pm0.48) \times 10^3$ $W \cdot m^{-1} \cdot K^{-1}$) and also the best conductor of electricity known (studies have shown electron mobility at values of more than 15,000 $cm^2 \cdot V^{-1} \cdot s^{-1}$). Other notable properties of graphene are its unique levels of light absorption at $\pi\alpha \approx 2.3\%$ of white light, and its potential suitability for use in spin transport. [17]

Carbon nanotubes (CNTs) are allotropes of carbon with a cylindrical nanostructure. CNTs were discovered by Sumio Iijima in 1991 [18]. Nanotubes have been constructed with length-to-diameter ratio of up to 132,000,000:1 [19]. These cylindrical carbon structures have unusual properties, which are valuable for nanotechnology, electronics, optics and other fields of materials science and technology. In particular, owing to their extraordinary thermal conductivity and mechanical and electrical properties, carbon nanotubes find applications as additives to various structural materials. [20]

Nanotubes are members of the fullerene structural family. Their name is derived from their long, hollow structure with the walls formed by one-atom-thick sheets of carbon, called

graphene. These sheets are rolled at specific and discrete ("chiral") angles, and the combination of the rolling angle and radius decides the nanotube properties; for example, whether the individual nanotube shell is a metal or semiconductor. Nanotubes are categorized as single-walled carbon nanotubes (SWCNTs) and multi-walled carbon nanotubes (MWCNTs). Individual nanotubes naturally align themselves into "ropes" held together by van der Waals forces, more specifically, π-stacking. The chemical bonding of carbon in CNTs is composed entirely of sp^2 bonds, similar to those of graphite. These bonds, which are stronger than the sp^3 bonds found in alkanes and diamond, provide nanotubes with their unique strength. [21]

2.2. Glass-like carbon electrodes

Glass-like (or vitreous) carbon is a non-graphitized carbon with a very high isotropy of its structural and physical properties and with a very low permeability for liquids and gases [22]. Glassy carbon (GC) is typically a hard solid prepared by heat-treatment at elevated temperatures (1000-3000 °C) of polymeric precursors such as co-polymer resins of phenol formaldehyde. Glass-like carbon combines glassy and ceramic properties with those of graphite. GC has a lower density (1.3-1.5 g cm^{-3}) than graphite (2.27 g cm^{-3}) or diamond (3.52 g cm^{-3}); this density reflects its porous microstructure. Glassy carbon has a sp^2 bonded atoms and fullerene-related structure (2-dimensional hexagonal lattice of carbon). [23]

The most important properties of GC are high temperature resistance, hardness (7 Mohs), low density, low electrical resistance, low friction, low thermal resistance, extreme resistance to chemical attack and impermeability to gases and liquids. Only oxygen above 600 °C and oxidants may attack vitreous carbon. Glassy carbon is widely used as an electrode material in electrochemistry, as well as for high temperature crucibles and as a component of some prosthetic devices, and can be fabricated as different shapes, sizes and sections. It resists strong acids and bases and is inert over a wide range of electrical potentials. GC is a useful electrode material, particularly where high current densities, low electrical/fluid flow resistance, minimal cell volume loss to electrodes and the ability to hold infused materials within controlled pore sizes are required. [24]

2.3. Cyclic voltammetry

Cyclic voltammetry (CV) is an electrochemical technique which measures the current that develops in an electrochemical cell under conditions where voltage is in excess of that predicted by the Nernst equation. CV is performed by cycling the potential of a working electrode, and measuring the resulting current. The current at the working electrode is plotted versus the applied voltage (i.e., the working electrode's potential) to give the cyclic voltammogram trace. Electrochemical system for CV measurements consists of an electrolysis cell, a potentiostat, a current-to-voltage converter, and a data acquisition system. The electrolysis cell consists of a working electrode, counter electrode, reference electrode, and electrolytic solution. The working electrode's potential is varied linearly with time, while the reference electrode maintains a constant potential. The counter electrode conducts electricity from the signal source to the working electrode. The purpose of the electrolytic solution is to provide ions to the electrodes during oxidation and reduction. A potentiostat is an electronic device, which uses a dc power source to produce a potential which can be maintained and accurately determined, while allowing small currents to be drawn into the system without changing the voltage. The current-to-voltage converter measures the resulting current, and the data acquisition system produces the resulting voltammogram. [25]

Cyclic voltammetry can be used to study qualitative information about electro-chemical processes under various conditions, such as the presence of intermediates in oxidation-reduction reactions, the reversibility of a reaction, etc. CV can also be used to determine the electron stoichiometry of a system, the diffusion coefficient of an analyte, and the formal redox potential, which can be used as an identification tool. In addition, because concentration is proportional to current in a reversible, Nernstian system, concentration of an unknown solute can be determined by generating a calibration curve of current vs. concentration. [26]

2.4. Oxygen reduction reaction

The oxygen reduction reaction (ORR) is a fundamental reaction in life processes such as biological respiration, and in energy converting systems such as fuel cells. It is a multielectron process that involves a number of elementary steps and various reaction intermediates. [1] Normally, the ORR kinetics is very slow. In order to speed up the ORR kinetics to reach a practical usable level in a fuel cell, a cathode ORR catalyst is needed. In acidic aqueous solution the reaction proceeds by either a four-electron pathway with water as final product:

$O_2 + 4H^+ + 4e^- \rightarrow H_2O$ $E^0 = 1.229$ V (1)

or through two-electron pathway with formation of hydrogen peroxide

$O_2 + 2H^+ + 2e^- \rightarrow H_2O_2$ $E^0 = 0.70$ V. (2)

Peroxide can be further reduced to water

$H_2O_2 + 2H^+ + 2e^- \rightarrow 2H_2O$ $E^0 = 1.76$ V (3)

In alkaline aqueous solution the corresponding reactions are:

$O_2 + 2H_2O + 4e^- \rightarrow 4OH^-$ $E^0 = 0.401$ V (4)

$O_2 + H_2O + 2e^- \rightarrow HO_2^- + OH^-$ $E^0 = -0.065$ V (5)

$HO_2^- + H_2O + 2e^- \rightarrow 3OH^-$ $E^0 = 0.867$ V. (6)

E^0 is the standard electrode potential at 25 °C. The pathways through 2- and 4-electron reduction have unique significance, depending on the applications. In fuel cell processes, the 4-electron direct pathway is highly preferred. The 2-electron reduction pathway is used in industry for H_2O_2 production. [1]. Figure 1 presents a general scheme for oxygen reduction in alkaline media. Some examples of electrocatalyst application for $2e^-$ and $4e^-$ reduction of oxygen reduction are given in Table 1.

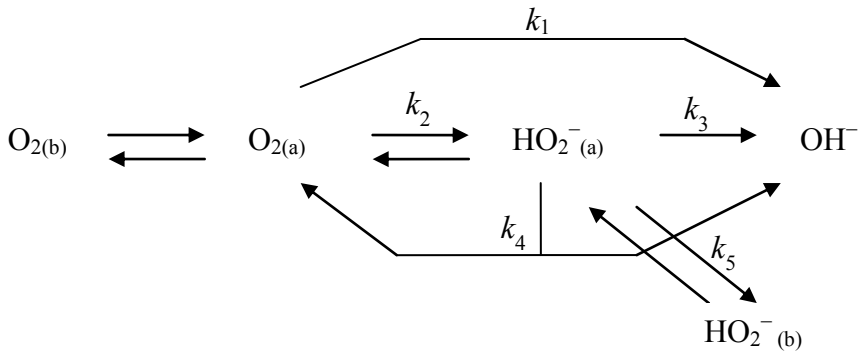

Figure 1. General scheme of ORR

Table 1. Electrocatalysts and their ORR pathway [31]

$2e^-$ reduction	$4e^-$ reduction
Mercury [27]	Platinum
GC	Pt/C
Graphene	Nitrogen-doped CNT [28]
VC	Silver in alkaline solution [29]
Undoped CNT	MnO_x/G
Sulfur modified Pt electrodes [30]	$AgMnO_x$/CNT

2.5. Rotating disk electrode studies

Rotating disk electrode (RDE) is one kind of the important and commonly used methods in electrochemistry particularly, in the fundamental understanding of electrochemical catalytic reaction mechanisms such as electrocatalytic ORR. The kinetics and mechanisms of the ORR catalyzed by both noble metal- and non-noble metal-based electrocatalysts are the most important aspects in fuel cell and other ORR-related electrochemical technologies. Using RDE to evaluate the activities of catalysts and their catalyzed ORR mechanisms is necessary and also one of the most feasible approaches in the development of ORR electrocatalysts. RDE has shown its advantages in measuring reaction electron transfer number, reactant concentration and diffusion coefficient, reaction rate constant, and reaction intermediates. [31]

This electrode is rather simple to construct and consists of a disk of the electrode material imbedded in a rod of an insulating material. For example, a commonly used form involves a platinum wire sealed in glass tubing with the sealed end ground smooth and perpendicularly to the rod axis. More frequently, the metal is imbedded into Teflon, epoxy resin, or another plastic. The shape of the insulating mantle is critical and that exact alignment of the disk is important, these factors are usually not troublesome in practice, except perhaps at high rotation rates, where turbulence and vortex formation may occur. It is more important that there is no leakage of the solution between the electrode material and the insulator. The rod is attached to a motor directly by a chuck or by a flexible rotating shaft or pulley arrangement and is rotated at a certain frequency (revolutions per second) [32].

2.6. Koutecky-Levich theory

The most popular theory for analyzing data collected using RDE for catalyzed ORR is called the Koutecky-Levich theory which gives the relationships among the ORR electron transfer number, O_2 concentration (or solubility), O_2 diffusion coefficient, viscosity of the electrolyte solution, and the electrode rotation rate. By analyzing these relationships, both the ORR kinetics and mechanism can be estimated, from which the activity of the electrocatalysts can be evaluated for further catalyst design and down-selection. Therefore, the O_2 concentration (or solubility), O_2 diffusion coefficient, and viscosity of the measuring electrolyte solution are the most frequently used parameters, and their values must be known in order to do the analysis by Koutecky-Levich theory.

The rotating disk electrode is a well characterized hydrodynamic electrode in which the transport, both diffusive and convective, is considered one-dimensional. Under steady-state conditions and considering the electrode process:

$$A + ne^- \rightarrow B \tag{7}$$

Sigmoidal voltammograms are expected with a steady-state limiting current I_{lim} expressed by the Levich equation:

$$I_{lim} = 0.62nFAD^{2/3}v^{-1/6}w^{1/2} \tag{8}$$

where w is the rotation speed (rad s^{-1}), v is the kinematic viscosity of the electrolyte (m^2 s^{-1}), D is the diffusion coefficient (m^2 s^{-1}) of the electroactive species of interest, A is the electrode area (m^2), F is the Faraday constant (96,485.34 C mol^{-1}) and n is the total number of electrons transferred per reacting species.

For an electrochemically irreversible reaction, the electrochemical rate constant (k) for reaction (7) is generally given by:

$$k = k^\circ \exp(-\frac{(n' + \alpha)FE}{RT}) \tag{9}$$

where R is the universal gas constant (J K^{-1} mol^{-1}), T is the temperature (K), α is the transfer coefficient and k° is the standard electrochemical rate constant ($m \cdot s^{-1}$) and n' is the number of electrons transferred before the rate-determining step. For the case of a flat

uniformly accessible rotating disk electrode, Koutecky and Levich proposed well-established procedure for the analysis of voltammetric data at variable rotation speeds [33].

For reactions which are controlled by both diffusion and kinetics at rotating disk electrodes, the total flux (j) of the reacting electroactive species is related to the speed of rotation of the electrode (ω) through Eq. (10), commonly known as the Koutecky–Levich equation:

$$\frac{1}{j} = \frac{1}{kc_{\infty}} + \frac{1}{DC_{\infty} / \chi_D} \tag{10}$$

where k is the potential dependent rate constant of the reaction defined by Eq. (9), c_{∞} is the bulk concentration of the reacting species in solution and χ_D is the thickness of the diffusion layer given by

$$\chi_D = 1.61 w^{-1/2} v^{1/2} D^{1/3} \tag{11}$$

Application of Eq. (10) to extract the kinetic parameters of an electrode reaction usually involves one of two common approaches. In the first case, the reciprocal of the measured current (I) where $I = –nFAj$, at selected potentials where the reaction is controlled by both diffusion and kinetic effects (diffusion–kinetic region) is plotted against the reciprocal of the square root of the electrode rotation rate, that is I^{-1} versus $\omega^{-1/2}$. From the slope of this graph, the number of electrons (n) involved in the charge transfer reaction can be calculated, and the intercept of the graph on the I^{-1} axis gives the kinetic current (I_k). Alternatively, and more commonly, I_k is calculated from the following expression:

$$I_k = \frac{I_{\text{lim}} \times I}{I_{\text{lim}} - I} \tag{12}$$

a reformulation of Eq. (10), where I_{lim} is the steady-state limiting current defined by Eq. (8). Knowing I_k, the rate constant k of the reaction at a given potential is then calculated from

$$I_k = nFAkc_{\infty} \tag{13}$$

I_k is commonly normalized to the electroactive surface area of the electrode, referred to as specific activity, or to the mass of the catalyst (mass activity), or rarely and specifically for non-platinum group metal catalysts, against the volume of the catalyst (volumetric activity) [34].

2.7. Silver-manganese oxide carbon supported catalysts

In last ten years Ag-MnO_x/C catalysts have received great interest in electrochemical community due to impressive interactions between silver nanoparticles and manganese oxide, which causes synergetic effect of the catalyst. For example, Zhang et al. [35] have shown synthesis of Ag-MnO_2/SWCNT by reducing $AgMnO_4$ with hydrazine and depositing onto the surface of carbon nanotubes. These catalyst have shown higher electrocatalytic activity for the oxygen reduction reaction and better performance for zinc air cell than Ag-MnO_x deposited onto mesocarbon microbeads (MCMB) and commercial graphite. The difference in electrocatalytic activities of the three electrodes may be attributed to the catalytic properties of the catalysts used with different carbon materials as supports. The (Ag + MnO_2)/SWCNT catalyst has a unique SWCNT entangled network structure dispersed uniformly with silver and manganese dioxide powders, which facilitates the oxygen contact with the catalyst and consequently leads to easy oxygen reduction.

Tang et al. [36] have demonstrated one-step synthesis method of carbon-supported Ag-MnO_x composites by $AgMnO_4$ pyrolysis at different temperatures. Among all the Ag-MnOx/C composites, Ag-Mn_3O_4/C obtained at 400 ◦C exhibits the highest activity toward the ORR. Vulcan XC-72R carbon black was used as the support material. Ag-Mn_3O_4/C electrocatalyst have shown great durability and higher ORR activity compared with Ag/C, Mn_3O_4/C and physically mixed Ag/C + Mn_3O_4/C suggesting a synergic effect between Ag and Mn_3O_4 and their ability to reduce produced peroxide to water. The influence of methanol on the ORR activities over both Ag/Mn_3O_4/C and Pt/C catalysts were evaluated in an O_2-saturated 0.1 M NaOH + 1 M CH_3OH solution. Ag-Mn_3O_4/C showed itself as advantageous cathode catalyst for DMFCs (Direct methanol fuel cells) since it avoids the negative effect of the methanol crossover from anodes.

Hu et al. [37] established a method for bifunctional catalysis of Ag–MnO_2/SWCNT by reduction route on the SWCNT surface. 5 wt% loadings of Ag–MnO_2 were found to be the best ratio for high catalytic activity. Kinetic activity of resulting electrocatalyst was compared with that of Ag–MnO_2 on acetylene black (AB) catalyst in terms of usage in zinc air batteries. The reaction at both composites is a direct four-electron process. It was considered that the different structure of the carbon supports effectively influenced the performance of the electrode. Nanotube structure is more advantageous for formation of a homogeneous composite and offers more effective active sites for oxygen reduction. The interwoven

network structure and the unique properties of SWCNT might facilitate the adsorption and catalytic reduction of molecular oxygen.

Lee et al. [38] presented method of reduced graphene oxide (rGO)-supported silver and manganese dioxide synthesis with sequential electrodeposition of MnO_x and Ag. The XRD and XPS data reveal that the MnO_x and Ag have been slightly alloyed and Mn presents with the dioxide form on rGO. As-prepared catalyst showed excellent electrocatalytic activity toward the ORR. O_2 was reduced directly to H_2O through a nearly four-electron pathway. This catalyst showed 1.2 times higher current density, much better anodic fuel tolerance and duration performance than that of 20 wt% Pt/C. Liu et al. [39] demonstrated synthesis of highly dispersed Ag and Mn_3O_4 nanoparticles coupled with carbon black through thermal decomposition. A possible formation mechanism for the Ag–Mn_3O_4/C composites can be explained as follows: Mn_3O_4 should be deposited homogeneously in the presence of the epoxyl and hydroxyl functional groups on surfaces of the carbon black modified by acidication in HNO_3. Subsequently, the obtained Mn_3O_4 domains dispersed over carbon serve as reduction centers for the formation of Ag particles. Ag ions can readily be reduced by domains of Mn_3O_4 with various valences including Mn (II), Mn (III) and Mn (IV) [40]. Ag–Mn_3O_4/C composite exhibits improved electrocatalytic activity and long-term stability compared to Ag/C (90 wt%). Such improvements can be associated with the formation of monolayer Ag_2O film, and active oxygen adsorption on the Ag surface.

Almost all Ag/Mn-based supported catalysts on a carbon substrate have demonstrated an overall increase in activity compared to the pure metal phases and the ORR proceeds through 4-electron pathway. Such electrocatalytic behavior could be assigned to the promotion of the direct 4-electron transfer by Ag and the rapid decomposition of peroxide ions by Mn. Also the decrease in d-band electrons in Ag would contribute to remarkably improved ORR activity. Moreover, the spillover of oxygen-containing species from the metal to the oxide due to the preferential adsorption of these species onto the oxide probably provides additional electrochemically active surface Ag sites for ORR, which is strongly suggested as another crucial factor for the enhancement of the ORR activity for the composite material. [41]

3. Experimental

3.1. Synthesis of Ag-MnO_x/C electrocatalyst

The graphene nanoplatelets (S_{BET} = 750 m^2 g^{-1}, an oxygen content of < 2 wt.% and a carbon content of >98 wt%) was purchased from Strem Chemicals, Inc. Multi-walled carbon nanotubes (MWCNTs, carbon content of >95 wt%) was bought from Nanolab, Inc. (Brighton, USA). All the other chemicals were of analytical reagent grade and used as received without any further treatment. All the aqueous solutions and suspensions used were prepared using Millipore ultrapure water (18.2 MΩ cm).

3.1.1. Preparation of Ag-MnO_x/G (electrodeposition method)

The manganese oxide nanoparticles were chemically deposited onto graphene surface as follows [42]: 0.12 g of graphene was mixed with a 2 mL of an aqueous solution containing 10 mM $MnSO_4$ (Aldrich). The suspension was maintained at 80 °C for 20 min under stirring, in order to allow impregnation of the graphene surface with manganese sulfate.

A 4 mL aqueous solution, containing 33 mmol of $KMnO_4$ (Merck) pre-heated to 80 °C was added to the suspension during vigorous stirring. Suspension was stirred for 15 min at 80 °C and then filtered and washed 3 times with water. Product was dried at 100 °C for 4 h.

Corresponding mass ratios in the obtained MnO_x/G material were 60 mg of graphene to 40 mg of Mn (60% graphene and 40% Mn). $MnSO_4$ is oxidized by the permanganate in the presence of graphene according to the following chemical reaction [24]:

$$2KMnO_4 + 3MnSO_4 + 2H_2O \rightarrow 5MnO_2 + 2H_2SO_4 + K_2SO_4 \quad (14)$$

For preparation of catalyst ink 10 mg of MnO_x/G was suspended in 4 mL of 0.5 wt.% Nafion (Aldrich) solution in ethanol by sonication for 15 min. 5 µL of this suspension was transferred to the polished glassy carbon (GC) electrode surface (A = 0.196 cm^2) by pipetting and dried for 5 min at 60 °C. Ag was electrodeposited onto MnO_x/G modified GC electrode surface from 1 mM $AgNO_3$ solution containing 0.1 M KNO_3. The electrodeposition experiments were carried out in a three-electrode cell with MnO_x/G modified GC as working electrode, Pt wire as counter electrode, and saturated calomel electrode (SCE) as a reference electrode. The potential of -0.5 V vs. SCE was applied for 30 s.

3.1.2. Preparation of Ag-MnO_x/CNT (dimethylformamide method)

Deposition of manganese oxide onto CNT surface has been provided by the same method, as for graphene described in subsection 3.1.1. Corresponding mass ratios in the obtained MnO_x/CNT material were 55 mg of graphene to 45 mg of Mn (55% graphene and 45% Mn). Silver nanoparticles were chemically attached to MnO_x/CNT as follows [43]: 50 mg of previously prepared MnO_x/CNT were added in 100 ml of dimethylformamide (DMF) solution and ultrasonically dispersed for 3 h to deagglomerate CNTs and form a uniform dispersed solution. 500 mg of $AgNO_3$ was then added to the solution and ultrasonically stirred again for another hour to attach silver to MnO_x/CNT particles. Final solution was filtered and washed with ethanol to remove excess of DMF. Product was dried at 75 °C overnight. Total mass of obtained Ag-MnO_x/CNT catalyst was 100 mg. For preparation of catalyst ink 10 mg of Ag-MnO_x/CNT was suspended in 4 mL of 0.5 wt.% Nafion (Aldrich) solution in ethanol by sonication for 15 min. 5 μL of this suspension was transferred to the polished GC electrode surface (A = 0.196 cm^2) by pipetting and dried for 5 min at 60 °C.

3.1.3. Preparation of Ag-MnO_x/CNT (simple method)

Prior to Ag and MnO_x deposition, CNT was pre-treated with concentrated nitric acid (14.6 M) at 120 °C for 4 h. Then, the treated carbon was filtered, washed by deionized water. Silver was chemically deposited onto MnO_x and CNT via straight synthesis as follows [40]: 100 mL of solution containing 0.1 M of $KMnO_4$ and 17 mL of $AgNO_3$ (0.1 M) were combined and stirred ultrasonically for 1 h. 0.1 g of CNT were dispersed in 11.7 mL of water by sonication, poured into previous solution and left to react for 30 min at 80 °C with vigorous mixing by magnetic stirrer. Then, the final solution was cooled to room temperature, filtered, washed 5 times with water, and dried at 75 °C in oven overnight. Corresponding mass of the obtained Ag-MnO_x/CNT catalyst was 145 mg. Catalyst ink preparation procedure was the same as described in subsection 3.1.2.

3.2. Surface morphology studies

For surface morphology studies Ag-MnO_x/G catalyst samples were prepared by modification of GC electrode with MnO_x/G powder suspension in 2-propanol (10 mg in 4 mL) followed by subsequent Ag electrodeposition. Ag-MnO_x/CNT catalyst samples were prepared by straight modification of catalyst powder suspension in 2-propanol. The presence of deposited Ag particles on MnO_x/C was confirmed by scanning electron microscopy (SEM). Energy-

dispersive X-ray spectroscopy (EDX) was used to quantitatively identify distribution of silver and manganese oxide particles on GC support surface. X-ray photoelectron spectroscopy (XPS) and X-ray fluorescence (XRF) techniques were applied to gain more information about the catalyst composition. The XPS measurements were performed with a SCIENTA SES-100 spectrometer using non-monochromatized Al Kα X-ray source (1486.6 eV), a take-off angle of 90° and a source power of 400 W. The pressure in the analysis chamber was less than 10^{-9} Torr. For collecting the survey spectra, the following parameters were used: energy range 600–0 eV, pass energy 200 eV, and step size 0.5 eV. In specific regions, high-resolution scans were performed with the pass energy of 200 eV and the 0.1 eV steps. The nominal Mn_2O_3 and Ag film thicknesses were measured by X-ray fluorescence spectrometer Rigaku ZSX 400 and program ZSX Version 5.55.meter Rigaku ZSX 400 and program ZSX Version 5.55.

3.3. Electrochemical measurements

The potential was applied with an Autolab potentiostat/galvanostat PGSTAT30 (EcoChemie B.V., The Netherlands) and the electrochemical experiments were controlled with the General Purpose Electrochemical System (GPES) software. Cyclic voltammetry (CV) tests were performed in a three-electrode glass cell, where reversible hydrogen electrode (RHE) was used as a reference electrode and a Pt foil as a counter electrode. The GC disk electrode coated with catalyst ink served as working electrode. GC disks (GC-20SS, Tokai Carbon) were pressed into a Teflon holder and were polished to a mirror finish with 1 and 0.3 μm alumina slurries (Buehler). After polishing the electrodes were sonicated in isopropanol and Milli-Q water for 5 min. Supporting electrolyte comprised 0.1 M aqueous KOH (p.a. quality, Merck) solution, which was saturated with Ar (99.999%, AGA) or O_2 gas (99.999%, AGA). Rotating disk electrode (RDE) measurements were carried out at various electrode rotation rates (ω) using RDE setup with CTV101 speed control unit and EDI101 rotator (Radiometer).

The RDE results of O_2 reduction were compared with those obtained with the bulk Ag and Pt electrodes under the same measurement conditions. The geometrical surface area of both bulk electrodes was 0.196 cm^2. The scan rate used for oxygen reduction and Ag dissolution experiments was 10 mV s^{-1}, and for stability testing 20 mV s^{-1}.

4. Results and discussions

4.1. Surface morphology and surface distribution of Ag-MnO_x/C catalyst

The SEM images of the unmodified graphene, MnO_x/G support and Ag-MnO_x/G catalyst are shown in Figure 2a, b and c, respectively. Aggregates of sub-micron graphene nanoplatelets with a diameter of <2 μm and a thickness of a few nanometers are clearly seen in Figure 2a. The surface morphology of the MnO_x/G support material is quite similar to that for pure graphene nanosheets, however, after local magnification thin layer of metal oxide distributed all over the graphene support can be distinguished. Figure 2c shows that the Ag particles for the Ag-MnO_x/G catalyst are the aggregates of the nanoparticles, which is about 12 nm. Meanwhile, the electrodeposited Ag nanoparticles are not distributed uniformly and some uncovered MnO_x/G support surface sites are present.

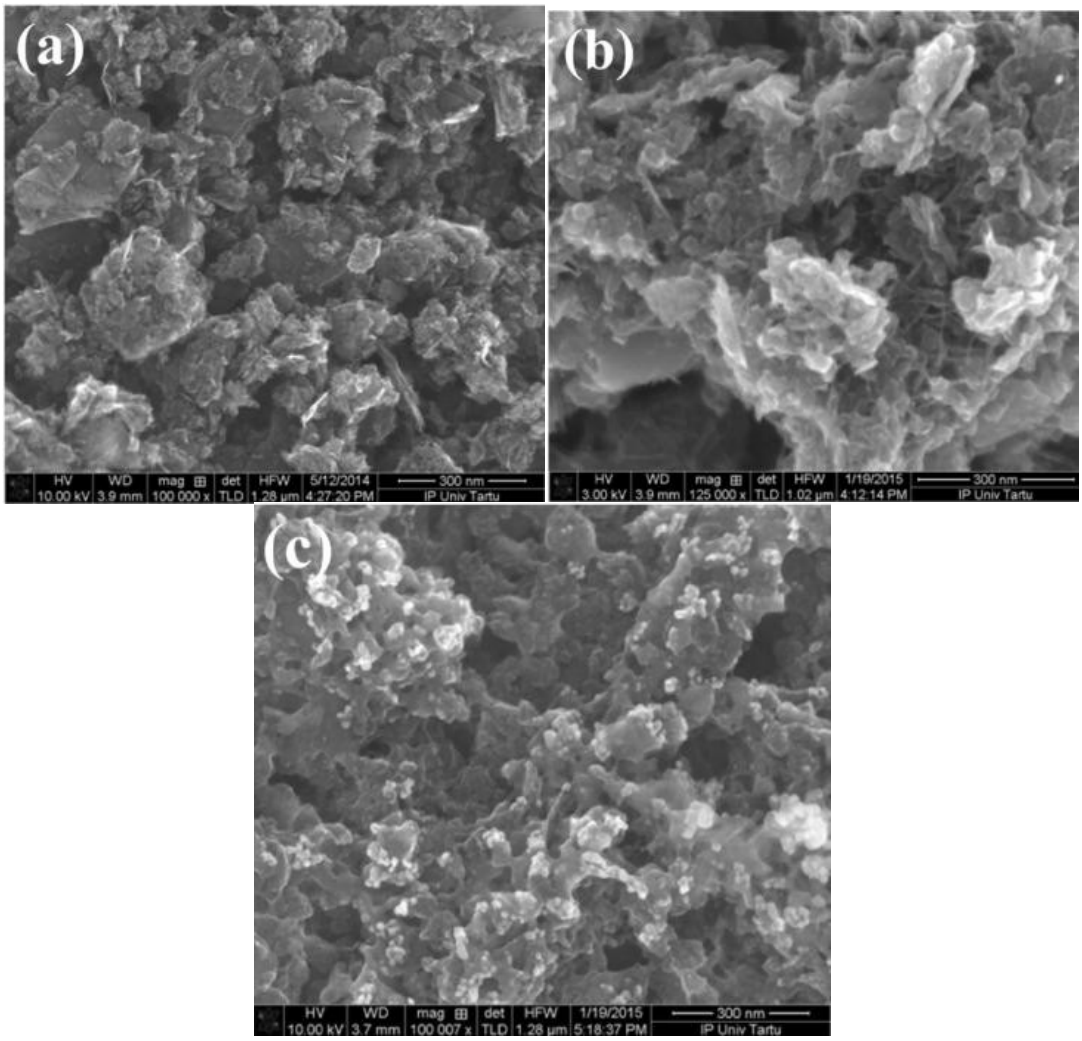

Figure 2. SEM images of (a) graphene, (b) MnO_x/G and (c) Ag-MnO_x/G modified GC electrodes at 300 nm magnification.

Figure 3a-d displays SEM images of CNT, MnO_x/CNT, Ag-MnO_x/CNT synthesized with DMF and simple method, respectively. MnO_x agglomerates attached to CNT can be identified in the center of Figure 3b. EDX beam, directed to that region reveals the presence of manganese oxide with the Mn/O ratio 1:2. Thus, the presence of MnO_2 can be assumed in the MnO_x/CNT and Ag-MnO_x/CNT composites. In Figure 3c and 3d much larger agglomerates are demonstrated. The EDX measurements expose the presence of silver in those regions.

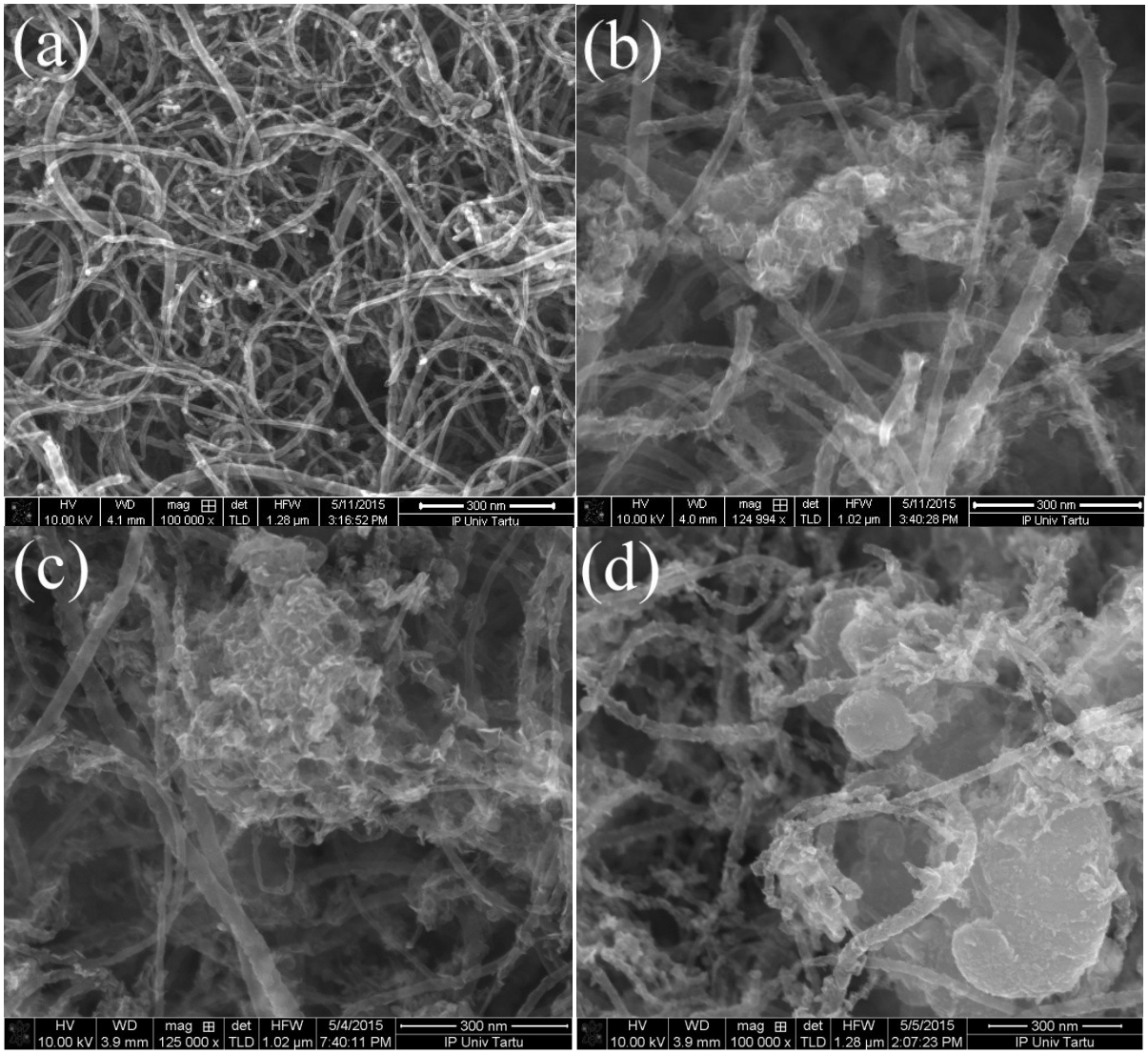

Figure 3. SEM images of (a) CNT, (b) MnO_x/CN, (c) Ag-MnO_x/CNT (DMF method of synthesis), (d) Ag-MnO_x/CNT (simple method) modified GC electrodes at 300 nm magnification.

The EDX measurements (Table 2) were performed to obtain information about the surface composition of Ag-MnO_x/C catalyst. According to the EDX results, all catalyst contains

almost equal amount of Mn (~20 wt%) and Ag (~30 wt%). Only Ag-MnO_x/CNT catalyst synthesized by DMF method has less amount of Ag (~25 wt%).

Table 2. EDX element distribution in the Ag-MnO_x/C catalysts surface (%)

Catalyst	C	O	Mn	Ag
Ag-MnO_x/graphene	27.81	21.45	18.97	31.77
Ag-MnO_x/CNT (DMF method)	36.81	19.68	19.25	24.06
Ag-MnO_x/CNT (simple method)	27.60	21.16	18.61	32.63

In order to further investigate the valence states of Mn and Ag on the surface of the prepared material, the XPS experiments were performed with the Ag-MnO_x/G, and the results are shown in Figure 4. The binding energies (BE) of $Mn2p_{3/2}$ and $Mn2p_{1/2}$ are 641.9 and 653.2 eV, respectively, which shows that manganese consists of a mixture of Mn^{3+} and Mn^{4+}. Although the average oxidation states of manganese cannot be determined from the analyses of Mn2p binding energies [44], still, the XPS spectra of O1s has three separate peaks at 528.8, 530.6, and 532.5 eV. These BE values can be attributed to three different types of oxygen bonding, where 528.8 eV corresponds to BE of oxygen bonded to manganese, 530.6 eV corresponds to activated oxygen adsorbed on the surface of the catalyst, and 532.5 eV corresponds to adsorbed water and −OH groups [45].

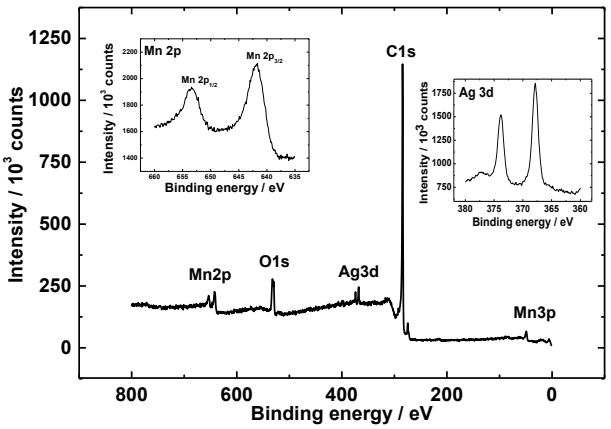

Figure 4. XPS spectra for Ag-MnO_x/G modified GC electrodes. Inset: high resolution XPS spectra in the Mn2p and Ag3d regions.

The Ag3d XPS peaks were also in evidence at BE values at 366.5 eV for $Ag3d_{5/2}$ and 372.5 eV for $Ag3d_{3/2}$, which are typical for Ag^{+} and Ag^{q+} clusters [46]. The XPS peaks of Ag observed in this research demonstrate that Ag is present in the zero-valent (metallic) state. [47, 48] Complimentary XRF measurements revealed that the Mn_2O_3 layer thickness was 9-10 nm, and the nominal thickness of Ag overlayer was 4 nm. The Mn/O mass ratios for Ag-MnO_x/G samples were 1.7, when theoretical mass Mn/O ratio for Mn_2O_3 is 2.29.

4.2. Cyclic Voltammetry

For the electrochemical characterization of the catalysts, the cyclic voltammetry (CV) curves for the Ag-MnO_x/G, Ag-MnO_x/CNT, MnO_x/G modified GC, bulk Ag and bulk Pt electrodes were recorded with a scan rate of 0.05 V s^{-1} in the potential range between 0.05 and 1.4 V in Ar-saturated 0.1 M KOH solution and presented in Figure 5. For all Ag-containing catalysts the cathodic silver surface oxide reduction peaks in the potential range between 1.0 and 1.2 V were evident. These cathodic peaks are assigned to the transformation of silver oxides to metallic silver and can be observed for Ag-MnO_x/G, Ag-MnO_x/CNT and Ag/G modified GC and bulk Ag electrodes. This peak for Ag-MnO_x/G and Ag-MnO_x/CNT catalysts is relatively weak, which is attributed to the lower amount of AgO formed. A pair of redox peaks observed at approximately 1.0 and 0.55 V, respectively, are associated with the formation of MnOOH from MnO_2 [49]

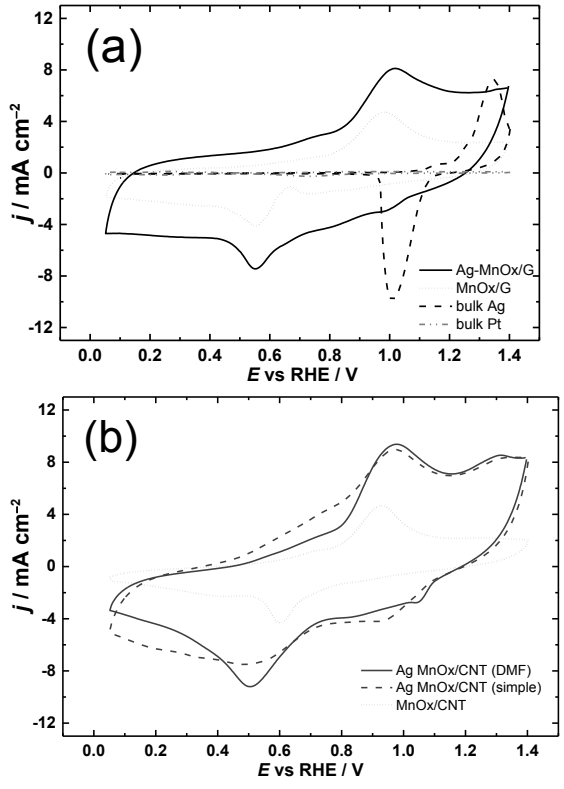

Figure 5. CV curves of Ag-MnO_x/G, MnO_x/G modified GC and bulk Pt and Ag electrodes (a); Ag-MnO_x/CNT, MnO_x/CNT (b) in Ar-saturated 0.1 M KOH solution, $\nu = 50$ mV s^{-1}.

For MnO_x/G modified GC electrode, another reduction peak was well-defined at approximately 0.7 V. It was previously stated that first the reduction of O_2 to HO_2^- takes place at approximately 0.7 V and the electrochemical transition of HO_2^- to OH^- takes place at more negative potentials [50].

4.3. Electrocatalytic activity toward the ORR

RDE measurements were performed to determine the predominant pathway of oxygen electroreduction. For the RDE experiments the pure Faradic current under O_2 was obtained by subtraction from the background current obtained under argon in the same voltammetry sweep condition. ORR polarization data recorded with the Ag-MnO_x/G and Ag-MnO_x/CNT (DMF and simple method) composite catalysts in 0.1 M KOH are shown in Figure 6, Figure 7a and b respectively.

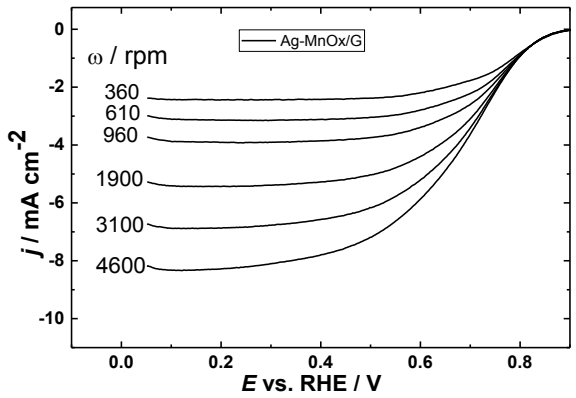

Figure 6. ORR polarization curves for Ag-MnO_x/G catalyst in O_2-saturated solution 0.1 M KOH solution at different electrode rotation speeds, $\nu = 10$m V s^{-1}.

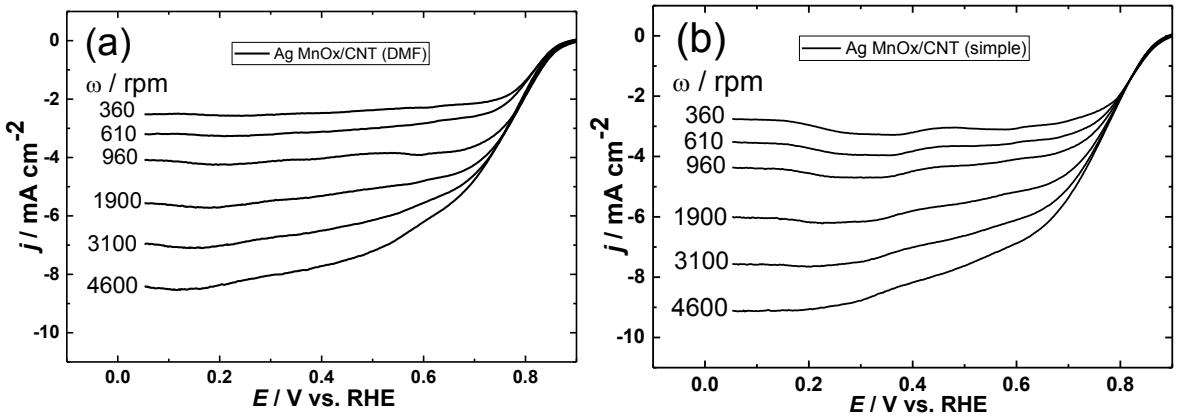

Figure 7. ORR polarization curves for Ag-MnO_x/CNT (DMF method) (a) and (simple method) (b) catalysts in O_2-saturated solution 0.1 M KOH solution at different electrode rotation speeds, $\nu = 10$ mV s^{-1}.

RDE results were analyzed using the Koutecky–Levich equation [51]:

$$\frac{1}{j} = \frac{1}{j_k} + \frac{1}{j_d} = -\frac{1}{nFkC_{O_2}^b} - \frac{1}{0.62nFD_{O_2}^{2/3}\nu^{-1/6}C_{O_2}^b\omega^{1/2}} \quad (15)$$

where j is the measured current density, j_k and j_d are the kinetic and diffusion-limited current densities, respectively; k is the electrochemical rate constant for O_2 reduction, D_{O_2} is the diffusion coefficient of oxygen (D_{O_2} = 1.9 × 10^5 cm^2 s^{-1} [52]), $C_{O_2}^b$ is its concentration in the bulk (1.2 × 10^{-6} mol cm^{-3} [52]) and ν is the kinematic viscosity of the solution (0.01 cm^2 s^{-1} [53]). These data are given for 0.1 M KOH solution.

The K–L plots of O_2 reduction on Ag-MnOx/C catalyst are shown in Figure 8, 9a and b. The K–L lines are parallel and the extrapolated lines yield intercepts other than zero indicating that the process of oxygen reduction is under the mixed kinetic–diffusion control in the range of potentials studied. The number of electrons transferred per O_2 molecule (n) was calculated from the slope of the K–L lines shown in Figure 8, Fig.9a and b. The value of n is close to four which approves that water is the final product of the reduction of O_2

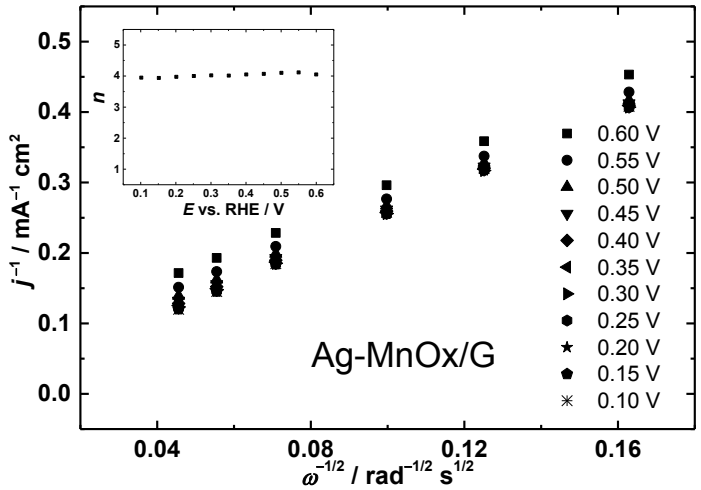

Figure 8. Koutecky–Levich plots for Ag-MnOx/G in 0.1 M KOH solution at different potentials. Inset: the potential dependence of n, calculated from the K-L plots.

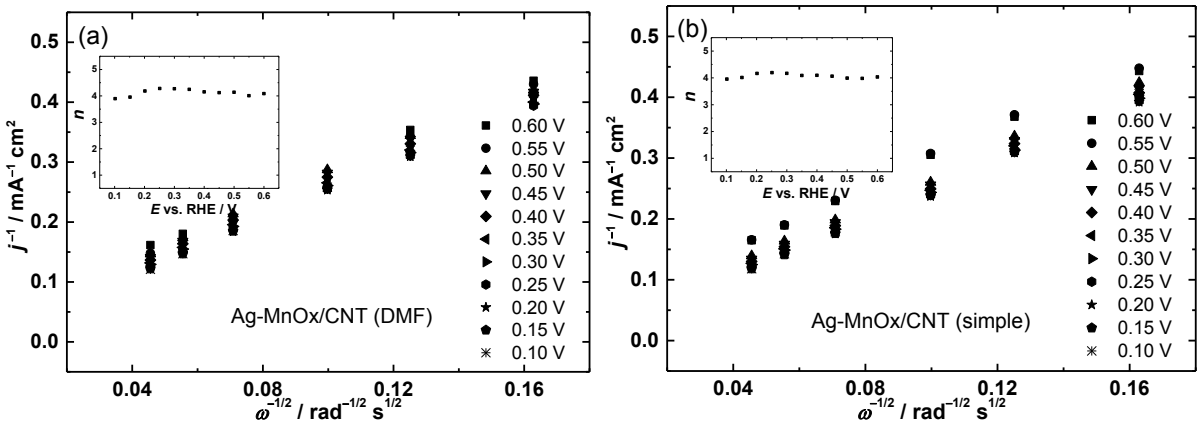

Figure 9. Koutecky–Levich plots for Ag-MnO_x/CNT (DMF method) (a) and (simple method) (b) in 0.1 M KOH solution catalysts at different potentials. Inset: the potential dependence of n, calculated from the K-L plots.

The electrocatalytic activity and diffusion current density values for all three Ag-MnO_x/C based composites are much higher than that of Ag/C and MnO_x/C composites due to the intrinsic synergy of silver and manganese oxide. The ORR limiting current density at 1900 rpm on Ag-MnO_x/C catalysts were approximately 5.51 mA cm^{-2} (Ag-MnO_x/G), 5.56 mA cm^{-2} (Ag-MnO_x/CNT DMF) and 6.02 mA cm^{-2} (Ag-MnO_x/CNT simple) which is similar to that of bulk Ag and higher than Ag/C and MnO_x/C composites (4.45 and 4.47 mA cm^{-2}, respectively), but slightly lower than that of the bulk Pt electrode (6.15 mA cm^{-2}). The onset potential for Ag-MnO_x/C catalysts was approximately 0.9 V, which is very close to that for bulk Pt (0.95 V). Two distinct Tafel slopes in two potential regions ($0.9>E>0.8$ V and $0.8>E>0.7$ V) were found for all catalyst under study. For Ag-MnO_x/C catalysts material the slope values were -0.057 and -0.122 V (Ag-MnO_x/G), -0.050 and -0.127 V (Ag-MnO_x/CNT DMF), -0.047 and -0.122 V (Ag-MnO_x/CNT simple), per decade at low and high overpotentials, respectively, which indicates that the ORR mechanism is similar to that on platinum. Wu et al. presented similar results for Ag−MnO_x/C composites, the Tafel slope values were about −55 and −120 mV at low and high overpotentials. [54] The comparable Tafel behavior for the electrodes studied was also obtained by Tang et al. indicating that the ORR mechanism is the same, where the one-electron transfer is the rate-determining step at low overpotentials and the two-electron transfer reaction is the rate-determining step at the higher overpotentials. [36]

The as-prepared Ag-MnO_x/C composites exhibits an onset potential of ~0.9 V and an overall 4-electron transfer involved in the ORR, indicating its potential application as the cathode

catalyst for alkaline membrane fuel cells. On the basis of the onset potential values, the intrinsic ORR activity of the Ag-MnO_x/C composites appears to be higher than that of the Ag catalyst.

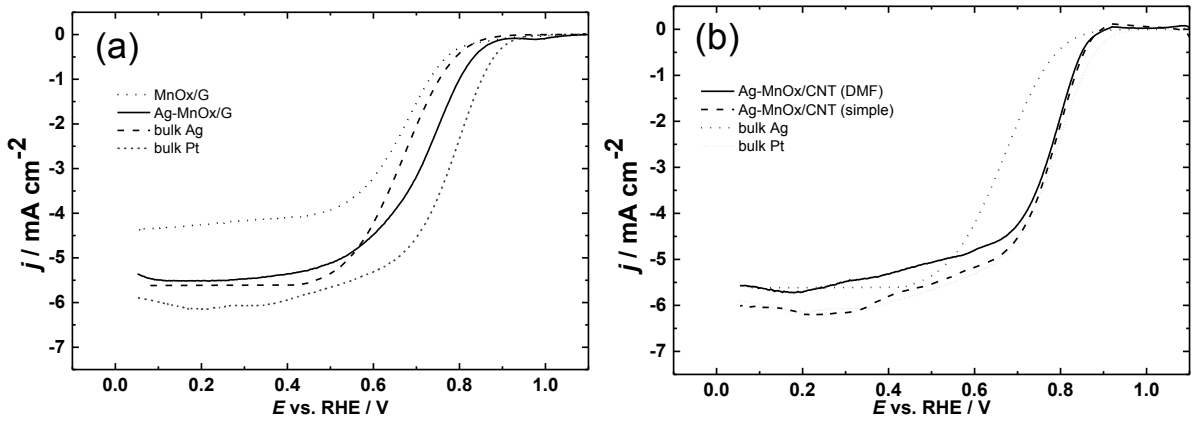

Figure 10. Comparison of the RDE results for MnO_x/G, Ag-MnO_x/G, bulk Ag, bulk Pt (a) and Ag-MnO_x/CNT (DMF and simple method), bulk Ag, bulk Pt (b) catalysts in O_2 saturated 0.1 M KOH, rotation speed: 1900 rpm, $\nu = 10$ mV s^{-1}.

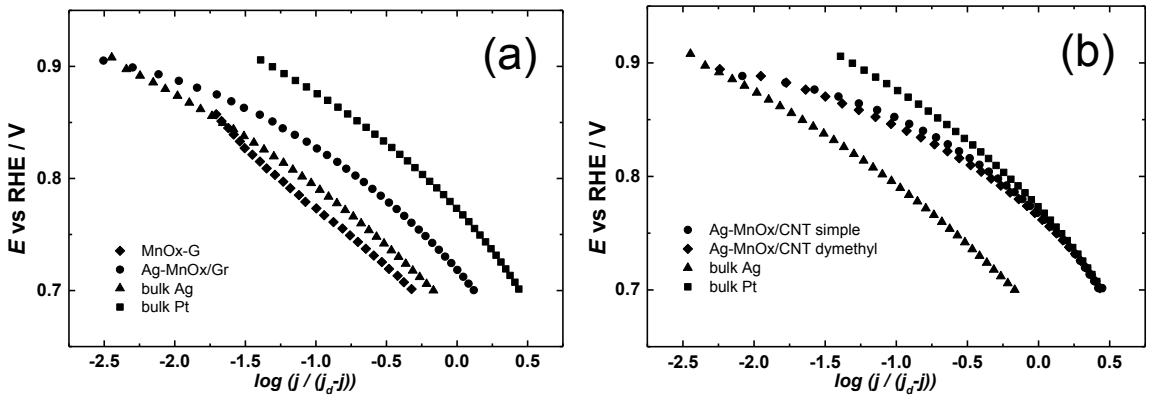

Figure 11. Comparison of Tafel plots for oxygen reduction on for MnO_x/G, Ag-MnO_x/G, bulk Ag, bulk Pt (a) and Ag-MnO_x/CNT (DMF and simple method), bulk Ag, bulk Pt (b) catalysts in O_2 saturated 0.1 M KOH, rotation speed: 1900 rpm, $\nu = 10$ mV s^{-1}.

Kinetic parameters of the electrocatalysts are listed in Table 3. The half-wave potential ($E_{1/2}$) value of Ag-MnO_x/CNT simple (0.77 V) and Ag-MnO_x/CNT DMF (0.76 V) is very near to bulk Pt (0.78 V), which can be also observed in Figure 10a and b. Such impressive electrocalytic activity of synthesized catalysts makes them auspicious candidates for non-platinum catalysts in alkaline media.

Table 3. Kinetic parameters for oxygen reduction on Ag-MnO_x/G, MnO_x/G, Ag-MnO_x/CNT (DMF and simple method), bulk Pt, and Ag electrodes.

Electrode	Tafel slope (V) *Region I	Tafel slope (V) *Region II	$E_{1/2}$ (V)
Ag-MnO_x/CNT (DMF)	-0.050	-0.127	0.76
Ag-MnO_x/CNT (simple)	-0.047	-0.122	0.77
Ag-MnO_x/G	-0.057	-0.122	0.72
MnO_x/G	-0.096	- 0.104	0.67
Bulk Pt	-0.055	-0.104	0.78
Bulk Ag	-0.085	-0.113	0.70

*Region I (0.90>*E*>0.8 V), region II (0.8>*E*>0.7 V)

The superior ORR activity of Ag-MnO_x/C catalysts could be explained by the introduction of Ag nanoparticles which may promote the adsorption of oxygen due to induced defects by forming Ag−O−Mn bonds. [45] Also, small distance between Ag and MnO_x particles may facilitate the formation of the strong particle-to-particle electronic interaction between two particles by way of the conductive carbon, thereby providing synergistic ligand and ensemble effects, acting as a bifunctional catalyst in ORR electrocatalysis. [39] Another source of enhanced ORR activity can be the spillover of oxygen-containing species from Ag surface sites to the neighboring MnO_x sites as a result of the preferential adsorption of these species onto the oxide. It is believed that the electron donation can increase the d-band vacancy of Ag and then subject the Ag atoms to a tensile force that narrows the d-orbital to generate an up-shifting of the d-band center of Ag [55]. Another source of such catalytic properties of Ag-MnO_x/C can be attributed to introduction of Ag nanoparticles. Manganese dioxide adsorbed the oxygen as shown in the following equation [56]:

$$MnOOH(s) + O_2(g) \leftrightarrow MnOOH^{\cdots}O_2(s) \quad (15)$$

$$MnO_2(s) + H_2O(l) + e\text{-} \leftrightarrow MnOOH(s) + OH^-(l) \quad (16)$$

$$MnOOH/O_2(s) + e^- \leftrightarrow MnO_2(s) + HO_2^-(l) \quad (17)$$

Therefore, the reactions in Eqs. (15)–(17) are equal to the Eqs. (5) and (6), which corresponds to the common knowledge that O_2 reduction occurs simultaneously with MnO_2 reduction. The oxygen reduction peak of the electrode with an Ag–MnO_x/C catalyst is because the insertion of a proton into MnO_2 as the Eqs. (15) and (16), the Eq. (17) no longer appears in this process, which then produces synergistic effect with Ag, and the adsorption of O_2 transfers from

MnOOH to the surface of Ag, which can be explained using the mechanism of reaction, as shown in the following equations:

$$MnOOH^{\cdots}O_2(s) + Ag(s) \leftrightarrow MnOOH(s) + Ag^{\cdots}O_2(s) \quad (18)$$

$$2Ag^{\cdots}O_2(s–g) + H_2O(l) + 2e^- \rightarrow Ag_2O(s) + 2HO_2^-(l) \quad (19)$$

Ag may further facilitate the electrochemical reduction of HO_2^- as Eq. (16), thus the total reaction mechanism of the electrode with Ag–MnO_x/C at -0.05 V is:

$$2Ag(s) + 2MnO_2(s) + 3H_2O(l) + 2O_2(g) + 4e^- \rightarrow$$

$$Ag_2O(s) + 2MnOOH(s) + 2OH^-(l) + 2HO_2^-(l) \quad (20)$$

The instability of Ag_2O and MnOOH, allows these elements easily decompose into Ag and MnO_2, which continue catalyze the ORR circularly. Thus, the catalyst of Ag–MnO_x/C catalyzes the overall reduction of O_2 to OH^- at -0.15 V. This result can be attributed to Eq. (20), which is equal to the combination of Eqs. (5) and (6) [55].

4.4. Degradation test of Ag-MnO_x/C catalysts

Long-term stability of the prepared catalyst is very important for its application in fuel cells. A repetitive potential cycling between 0.05 and 1.3 V was applied to investigate the stability of the Ag-MnO_x/C composites toward the ORR. Figures 12, 13a and b show the ORR polarization curves recorded before and after 1000 potential scans. Proximity of these RDE voltammetry curves indicates a high stability of the catalyst studied. The $E_{1/2}$ value of Ag-MnO_x/C decreased for less than 50 mV for each catalyst after the long-term cycling under harsh electrochemical conditions. All the Ag-MnO_x/C catalysts revealed itself as a stable electrocatalyst for ORR. Inset of Figures 12, 13a and b represents a pattern of CV curves during 1000 cycles. With the scanning cycle number further increasing, the positions of the characteristic peaks in the CV curves have no obvious shift with the peaks intensity. After each 100 cycles the area under the CV peak changes fractionally but insignificantly. As indicated by the CVs, the Ag-MnO_x/C catalysts showed no loss in silver oxide reduction current and maintained significant durability during repeat potential cycling. Figure 14 displays comparison of the catalysts activity toward the ORR after 1000 cycles. Ag-MnO_x/CNT (simple) electrocatalyst remains the most active even after degradation tests, compared to Ag-MnO_x/CNT (DMF) and Ag-MnO_x/G.

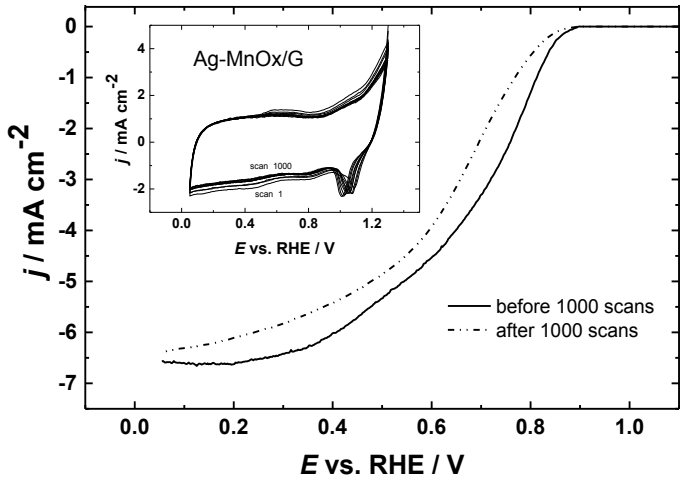

Figure 12. Comparison of the RDE polarization curves of oxygen reduction for Ag-MnO_x/G catalyst before and after 1000 scans in O_2-saturated 0.1 M KOH, ν = 10 mV s^{-1}, and rotation speed: 1900 rpm. Inset: CV curves for degradation test of Ag-MnO_x/G modified GC electrode in Ar-saturated 0.1 M KOH, ν = 50 mV s^{-1}.

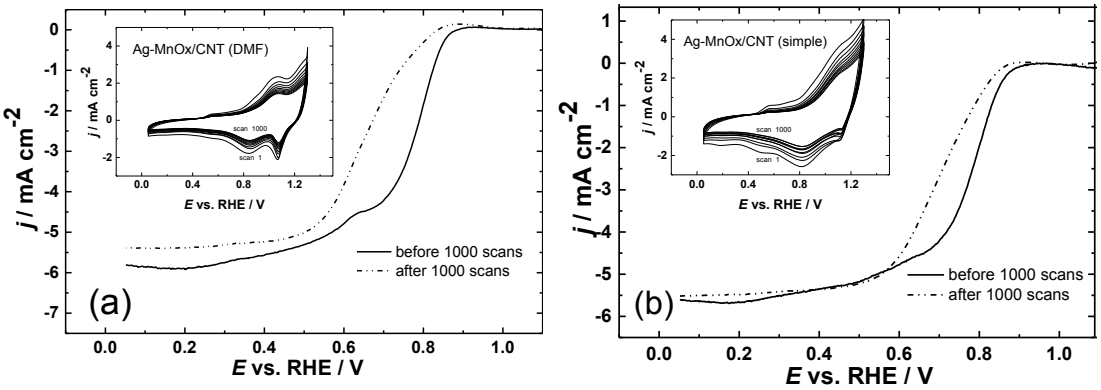

Figures 13. Comparison of the RDE polarization curves of oxygen reduction for Ag-MnO_x/CNT (DMF) (a) and Ag-MnO_x/CNT (simple) (b) modified GC electrode before and after 1000 scans in O_2-saturated 0.1 M KOH, ν = 10 mV s^{-1} and rotation speed: 1900 rpm. Inset: CV curves for degradation test of Ag-MnO_x/CNT modified GC electrodes in Ar-saturated 0.1 M KOH, ν = 50 mV s^{-1}.

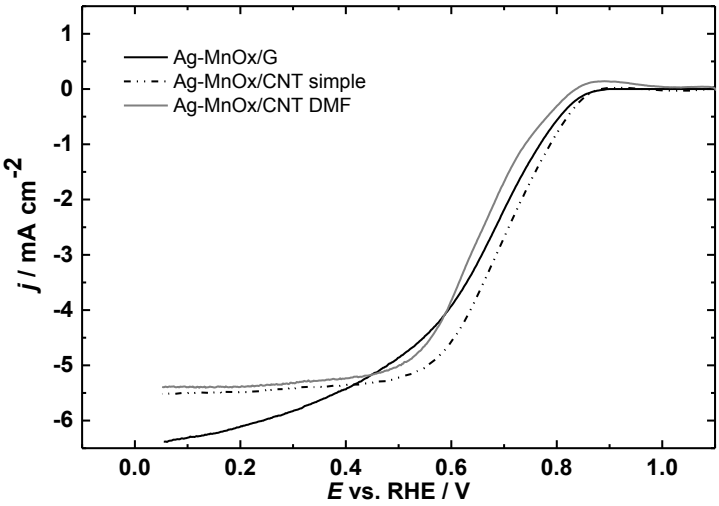

Figure 14. Comparison of the RDE polarization curves of oxygen reduction for Ag-MnO_x/C modified GC electrode after 1000 scans in O_2-saturated 0.1 M KOH, ν = 10 mV s^{-1}, and rotation speed: 1900 rpm.

High durability of Ag-MnO_x/C catalysts can be related to ability to minimize the formation of H_2O_2. Two possible reasons for the low HO_2^- production may be deduced from the unique morphological and electronic structures of the composite material. On the one hand, as the strong electron transfer from carbon to the MnO_x is observed, the resulting positively charged surfaces on the adjacent C atoms would establish favorable sites for the side-on O_2 surface adsorption and facilitate the direct reduction of oxygen to OH^- via a four-electron process. [57] On the other hand, these highly dispersed and nanoscale Ag and MnO_x particles with close proximity to each other (approximately <2–3 nm) can provide an ensemble effect, acting as a bifunctional catalyst, where these different particles complement each other by catalyzing different ORR reaction steps (four- and two-electron reductions), according to previous results for metal–metal oxide composites for ORR. [40] In this way, the HO_2^- intermediate generated on the Mn_3O_4 surfaces can easily diffuse to the neighboring Ag surfaces or the Ag–MnO_x interface, where it can undergo prompt disproportionation into OH^- and O_2 for further oxygen reduction with this hybrid catalyst. [39] Among the formation of H_2O_2, another reason of activity lost for Ag-MnO_x/C catalysts can be related to the formation of manganese carbonates and their sizes significantly increase to a few nm. In addition their dispersion over the carbon surface is no longer homogeneous. Moreover, the carbon-supported Ag-MnO_x nanoparticles are attacked by the alkaline solution. Manganite (Mn^{III}) is soluble in alkaline solution, whereas carbon and silver should be immune. Dissolution of Mn^{III} (which confers good ORR activity) implicating the decrease of overall electrocatalyst activity. [58]

5. Uncertainty estimation

Approximate number of electrons taking part in the oxygen reduction reaction was evaluated by same method, used in subsection 4.4. Uncertainty for number of electrons was calculated by single-lab validation approach, also known as Nordtest approach [59]. The main equation of the approach is:

$$u_c = \sqrt{u(R_w)^2 + u(bias)^2} \tag{16}$$

In Eq. (16) $u(R_w)$ is within-lab reproducibility component of uncertainty and $u(bias)$ is uncertainty component taking into account possible bias. Within-lab reproducibility were calculated from pooled within-day standard deviations; $u(bias)$ consists of next components:

$$u(bias) = \sqrt{RMS_{bias}{}^2 + u(C_{ref})^2} \tag{17}$$

where RMS_{bias} is bias between values of the reference material (RM) and the catalyst; $u(C_{ref})$ is uncertainty of RM. We have used MnO_x/G as RM because the ORR process on manganese oxides also proceeds via 4-electron pathway.

For uncertainty estimation, results from 3 different days for each synthesized composite material have been taken. Deviations of electron transfer numbers (n) are due to the preparation of the catalyst, especially pipetting of the catalytic material onto electrode surface. Also such deviations are caused by high porosity of carbon supported material, not perfectly flat surface of electrode decorated with electrocatalyst. Another source of uncertainty can be the formation of insignificant amount of H_2O_2 which is guiding ORR via 2-electron process or increase of particle size. All corresponding data for uncertainty estimation are presented in Table 3. Relative expanded uncertainties are 14% (Ag-MnO_x), 12% (Ag MnO_x/CNT DMF) and 11% (Ag MnO_x/CNT simple), respectively. Uncertainty is for the all components lower than 15% from the final value, which is acceptable in this kind of measurements.

Table 3. Uncertainty calculation for the Ag-MnO_x/C composites

data/composite		RM	Ag-MnOx/G			Ag-MnOx/CNT (DMF)			Ag-MnOx/CNT (simple)		
			3.03.2014	25.06.2014	30.10.2014	20.04.2015	28.04.2015	10.05.2015	28.04.2015	30.04.2015	5.05.2015
#	E,V	n_{RM}	n_1	n_2	n_3	n_1	n_2	n_3	n_1	n_2	n_3
1	0.50	3.98	4.36	4.69	4.10	4.15	4.14	3.89	4.17	4.33	3.99
2	0.45	3.97	4.29	4.64	4.07	4.30	4.12	3.94	3.98	3.96	4.06
3	0.40	3.94	4.22	4.61	4.05	4.26	4.15	3.91	4.15	4.21	4.10
4	0.35	3.91	4.15	4.57	4.01	4.16	4.25	3.95	4.07	4.25	4.09
5	0.30	3.91	4.11	4.57	4.02	4.26	4.27	4.12	4.16	4.18	4.17
6	0.25	3.93	4.05	4.55	4.00	4.16	4.28	4.22	4.26	4.22	4.20
7	0.20	3.92	3.95	4.52	3.97	4.06	4.19	4.23	4.24	4.04	4.17
8	0.15	3.96	3.82	4.48	3.94	4.21	3.96	4.15	4.35	4.23	4.01
9	0.10	4.00	3.62	4.49	3.95	4.21	3.90	4.29	4.40	4.20	3.95
average		3.95	4.06	4.57	4.01	4.19	4.14	4.08	4.18	4.20	4.08
st. dev.		0.03	0.07	0.24	0.05	0.07	0.13	0.16	0.11	0.13	0.09
P-d st.dev			0.29			0.26			0.22		
ubias		0.04									
Final result (95% k=2, norm)			n=4.22 +- 0.58			n=4.14 +- 0.51			n=4.15 +- 0.45		
Relative uncertainty			14%			12%			11%		

6. Conclusions

Three different methods for synthesis of Ag-MnO_x/C nanocomposites has been successfully shown. Surface morphology studies were provided to display catalyst nanostructure. All prepared silver-based catalysts demonstrated higher electrocatalytic activity for ORR than bulk Ag catalyst. The oxygen reduction reaction on the prepared catalyst proceeds via four-electron transfer pathway in alkaline media, avoiding the formation of hydrogen peroxide. Ag-MnO_x/C revealed sufficient stability after degradation tests. Synergetic effect between inexpensive metal (Ag) and metal oxide (MnO_x) have been achieved. Manganese oxide coupled with carbon-supported silver nanocatalyst demonstrate itself as promising candidate for non-platinum catalysts in alkaline media.

7. Summary

Manganese oxide coupled with carbon-supported silver nanocatalyst (Ag-MnO_x/C) was prepared with 3 different methods by chemical and electrochemical deposition. The physical properties and composition of the prepared Ag-MnO_x/C catalysts were investigated by X-ray photoelectron spectroscopy (XPS), scanning electron microscopy (SEM), as well as X-ray fluorescence (XRF) techniques and the catalytic activity toward the oxygen reduction reaction (ORR) in alkaline media was studied using cyclic voltammetry (CV) and the rotating disk electrode (RDE) method. The onset potential and the half-wave potential of the ORR on the prepared catalyst materials shifted positively compared to those of the bulk Ag electrode. Koutecky-Levich analysis revealed that the ORR predominant pathway was the 4-electron reduction, yielding less peroxide as an intermediate. After 1000 potential cycles between 0.05 and 1.3 V for accelerated aging tests, high catalytic stability of the Ag-MnO_x/C catalyst toward the ORR was observed, with the half-wave potential of the ORR shifting negatively only about 0.05 V.

8. Kokkuvõte

Hõbeda nanoosakestega kaetud mangaandioksiid seondati suurepinnalisele süsinikmaterjalile (Ag-MnO_x/C) kasutades kolme erinevat sünteesimeetodit. Ag-MnO_x/C katalüsaatori füüsikalisi omadusi ja koostist uuriti kasutades röntgenfotoelektronspektroskoopia, skaneeriva elektronmikroskoopia ning fluorestsensspektroskoopia meetodeid ja valmistatud katalüsaatorite elektrokatalüütilist aktiivsust hapniku elektrokeemilisel redutseerumisel uuriti tsüklilise voltamperomeetria ning pöörleva ketaselektroodi meetoditel 0,1 M KOH lahuses. Hapniku redutseerumise poollainepotentsiaal sünteesitud katalüsaatormaterjalidel nihkus positiivses suunas võrreldes kompaktse Ag-elektroodiga. Koutecky-Levichi analüüsi tulemustest selgus, et hapniku redutseerumine Ag-MnO_x/C katalüsaatoritel toimub peamiselt 4-elektronilise protsessina, mille käigus tekib väikeses koguses vesinikperoksiidi. Pärast pikaajalist potentsiaali tsükleerimist (1000 tsüklit potentsiaalide vahemikus 0,05 ja 1,3 V) jäi Ag-MnO_x/C katalüsaatormaterjali elektrokatalüütiline aktiivsus küllaltki stabiilseks (hapniku redutseerumise poollainepotentsiaali väärtus vähenes kõigest 0,05 V võrra).

9. References

[1] C. Song, J. Zhang, PEM fuel cell electrocatalyst and catalyst layers. Fundamentals and Applications, Springer-Verlag, London, 2008, pp. 9-91.

[2] H. Gasteiger, S. Kocha, B. Sompalli, F. Wagner. Activity Benchmarks and Requirements for Pt, Pt-Alloys, and Non-Pt Oxygen Reduction Catalysts for PEMFCs. Appl. Catal. B 56 (2005) 9-35.

[3] G. Wu, P. Zelenay, Nanostructured Nonprecious Metal Catalysts for Oxygen Reduction Reaction. Acc. Chem. Res. 46 (2013) 1878–1889.

[4] M. Vikkisk, I. Kruusenberg, U. Joost, E. Shulga, I. Kink, K. Tammeveski, Electrocatalytic oxygen reduction on nitrogen-doped graphene in alkaline media. Appl. Catal. B 147 (2014) 369-376.

[5] T. Schilling, M. Bron, Oxygen reduction at Fe–N-modified multi-walled carbon nanotubes in acidic electrolyte. Electrochim. Acta 53 (2008) 5379-5385.

[6] Y. Yuan, S. Zhou, Polypyrrole/carbon black composite as a novel oxygen reduction catalyst for microbial fuel cells. J. Power Sources 195 (2010) 3490-3493.

[7] N. Ominde, N. Bartlett, X.-Q. Yang, D. Qu, The effect of oxygen reduction on activated carbon electrodes loaded with manganese dioxide catalyst. J. Power Sources 185 (2008) 747-753.

[8] C.-C. Yang, S.-T. Hsu, W.-C. Chien, M.C. Shih, S.-J. Chiu, K.-T. Lee, C.L. Wang, Electrochemical properties of air electrodes based on MnO2 catalysts supported on binary carbons, Int. J. Hydrogen Energy 31 (2006) 2076-2081.

[9] A. Garcia, F. Lima, E. Ticianelli, M. Chatenet, Carbon-supported nickel-doped manganese oxides as electrocatalysts for the oxygen reduction reaction in the presence of sodium borohydride. J. Power Sources 222 (2013) 305–312.

[10] W. Sun, A. Hsu, R. Chen, Palladium-coated manganese dioxide catalysts for oxygen reduction reaction in alkaline media. 196 (2011) 4491-4498.

[11] F. Cheng, J. Shen, W. Ji, Z. Tao, J. Chen, Selective Synthesis of Manganese Oxide Nanostructures for Electrocatalytic Oxygen Reduction. ACS Appl. Mater. Interfaces 1 (2009) 460–466.

[12] L. Tammeveski, H. Erikson, A. Sarapuu, J. Kozlova, P. Ritslaid, V. Sammelselg, K. Tammeveski, Electrocatalytic oxygen reduction on silver nanoparticle/multi-walled carbon nanotube modified glassy carbon electrodes in alkaline solution. Electrochem. Commun. 20 (2012) 15–18.

[13] J. Guo, A. Hsu, D. Chu, R. Chen, Improving oxygen reduction reaction activities on carbon-supported Ag nanoparticles in alkaline solutions. J. Phys. Chem. C 114 (2010) 4324. 4330.

[14] J.-J. Han, N. Li, T.-Y. Zhang, Ag/C nanoparticles as an cathode catalyst for a zinc-air battery with a flowing alkaline electrolyte. J. Power Sources 193 (2009) 885-889.

[15] V. Georgakilas, Functionalization of Graphene, Wiley-VCH, Weinheim, 2014.

[16] A. Ivanovskii, A. Enyashin. Graphene-like transition-metal nanocarbides and nanonitrides. Russ. Chem. Rev, 82 (2013) 735-746.

[17] J. Fuente. The Properties of Graphene. http://www.graphenea.com/pages/graphene-properties#.VRGNCPmUfuQ recently updated 1.03.2015,

[18] S. Iijima, Helical microtubules of graphitic carbon. Nature 354 (1991) 56–58.

[19] X. Wang, Q. Li, J. Xie, Z. Jin, J. Wang, Y. Li, K. Jiang, S. Fan, Fabrication of Ultralong and Electrically Uniform Single-Walled Carbon Nanotubes on Clean Substrates. Nano Lett. 9 (2009) 3137–3141.

[20] S. Gullapalli, M.Wong, Nanotechnology: A Guide to Nano-Objects. Chem. Eng. Prog. 5 (2011) 28–32.

[21] D. Guldi, N. Martin, Carbon Nanotubes and Related Structures: Synthesis, Characterization, Functionalization, and Applications. Wiley-VCH, Weinheim, 2010.

[22] A. McNaught, A. Wilkinson, IUPAC Compendium of Chemical Terminology, Royal Society of Chemistry, Cambridge, 1997, p. 490.

[23] O. Schueller, S. Brittain, Fabrication and Characterization of Glassy Carbon MEMS. Chem. Mater. 9 (1997) 1399-1406.

[24] D. Sawyer, A. Sobkowiak, J. Roberts, Jr. Electrochemistry for Chemists, John Wiley and Sons, New York, 1995, p. 467.

[25] P. Kissinger, W. Heineman, Cyclic Voltammetry. J. Chem. Educ. 60 (1983) 702.

[26] H. Strobel, W. R. Heineman, Chemical Instrumentation: A Systematic Approach. 3rd Ed., John Wiley & Sons, New York, 1989.

[27] C.J. Van Velzen, M. Sluyters-Rehbach, A.G. Remijnse, G.J. Brug, J.H. Sluyters, The electrochemical reduction of oxygen to hydrogen peroxide at the dropping mercury electrode: Part I. Its kinetics at 6.5 pH<12.5 J. Electroanal. Chem. Interfacial. Electrochem. 134 (1982) 87-100.

[28] C. Xiong, Z. Wei, B. Hu, S. Chen, L. Li, L. Guo, W. Ding, X. Liu, W. Ji, X. Wang, Nitrogen-doped carbon nanotubes as catalysts for oxygen reduction reaction. J. Power Sources 215 (2012) 216-220.

[29] B. Blizanac, P. Ross, N. Markovic, Oxygen Reduction on Silver Low-Index Single-Crystal Surfaces in Alkaline Solution: Rotating Ring DiskAg(hkl) Studies. J. Phys. Chem. B 110 (2006) 4735-4741.

[30] S. Marcotte, D. Villers, N. Guillet, L. Roué, J.P. Dodelet, Electroreduction of oxygen on Co-based catalysts: determination of the parameters affecting the two-electron transfer reaction in an acid medium. Electrochim. Acta 50 (2004) 179–188.

[31] W. Xing, G. Yin, J. Zhang. Rotating Electrode Methods and Oxygen Reduction Electrocatalysts. 1st Ed, Elsevier, Walthman, 2014.

[32] A. J. Bard, L. R. Faulkner, Electrochemical Methods: Fundamentals and Applications. 2nd ed., John Wiley and Sons, New York, 2001, pp. 56-70.

[33] J. Koutecky, V. Levich, The use of a rotating disk electrode in the studies of electrochemical kinetics and electrolytic processes. Zh. Fiz. Khim. 32 (1958) 592-597.

[34] F. Jaouen, E. Proietti, M. Lefèvre, R. Chenitz, J. Dodelet, G. Wu, H. Chung, C. Johnston, P. Zelenay, Recent advances in non-precious metal catalysis for oxygen reduction reaction in polymer electrolyte fuel cells. Energy Environ. Sci. 4 (2011) 114-130.

[35] G.Q. Zhang, X.G. Zhang, Y.G. Wang, A new air electrode based on carbon nanotubes and Ag-MnO2 for metal air electrochemical cells. Carbon 42 (2004) 3097-3104.

[36] Q. Tang, L. Jiang, J. Qi, Q. Jiang, S. Wang, G. Sun, One step synthesis of carbon-supported Ag/MnyOx composites for oxygen reduction reaction in alkaline media. Appl. Catal. B 104 (2011) 337–345.

[37] F. Hu, X. Zhang, F. Xiao, J. Zhang, Oxygen reduction on Ag–MnO_2/SWNT and Ag–MnO_2/AB electrodes. Carbon 43 (2005) 2931–2936.

[38] K. Lee, M. Shamsuddin, S. Jeon, Electrochemical deposition of silver on manganese dioxide coated reduced graphene oxide for enhanced oxygen reduction reaction. J. Power Sources 288 (2015) 261-269.

[39] J. Liu, J. Liu, W.Song, F.Wang, Y. Song, The role of electronic interaction in the use of Ag and Mn3O4 hybrid nanocrystals covalently coupled with carbon as advanced oxygen reduction electrocatalysts. J. Mater. Chem. 2 (2014) 17477–17488.

[40] D. Slanac, A. Lie, J. Paulson, K. Johnston, K. Stevenson, Bifunctional Catalysts for Alkaline Oxygen Reduction Reaction via Promotion of Ligand and Ensemble Effects at Ag/ MnOx Nanodomains. J. Phys. Chem. C 116 (2012) 11032-11039.

[41] Z. Awaludin, M. Suzuki, J. Masud, T. Okajima, T. Ohsaka, Enhanced electrocatalysis of oxygen reduction on Pt/TaO_x/GC, J. Phys. Chem. C. 115 (2011) 25557-25567.

[42] I. Roche, K. Scott, Carbon-supported manganese oxide nanoparticles as electrocatalysts for oxygen reduction reaction in neutral solution. J. Appl. Electrochem. 39 (2009) 197–204.
[43] V. Rangari, G. Mohammad, S. Jeelani, A. Hundley, K. Vig, S. Singh, S. Pillai, Synthesis of Ag/CNT hybrid nanoparticles and fabrication of their Nylon-6 polymer nanocomposite fibers for antimicrobial applications. Nanotechnology 21 (2010) 95-102.
[44] Huang, H. Meng, Y. Labonte, A. Dobley, A. Suib, S. L., Large-Scale Synthesis of Silver Manganese Oxide Nanofibers and Their Oxygen Reduction Properties, J. Phys. Chem. C, 2013, 117 (48), 25352-25359.
[45] H. Huang, Y. Meng, A. Labonte, A. Dobley, S.L. Sui, Large-Scale Synthesis of Silver Manganese Oxide Nanofibers and Their Oxygen Reduction Properties. J. Phys. Chem. 117 (2013) 25352-25359.
[46] L. Sun, Q. Cao, B. Hu, J. Li, J. Hao, G. Jing, X. Tang, Synthesis, characterization and catalytic activities of vanadiumcryptomelane manganese oxides in low-temperature NO reduction with NH3. Appl. Catal. B. 393 (2011) 323−330.
[47] Y.Z. Zhou, J. Yang, T.T. He, H.F. Shi, X.N. Chen, Y.X. Lu, Highly Stable and Dispersive Silver Nanoparticle–Graphene Composites by a Simple and Low-Energy-Consuming Approach and Their Antimicrobial Activity. Small 9 (2013) 3445–3454.
[48] A. M. Ferraria, S. Boufi, N. Battaglini, A.M. B. Rego, M. Reivilar, Hybrid Systems of Silver Nanoparticles Generated on Cellulose Surfaces. Langmuir 26 (2010) 1996–2001.
[49] F. Lima, M. Calegaro, E. Ticianeli, Electrocatalytic Properties of PtCo/C and PtNi/C Alloys for the Oxygen reduction reaction in Alkaline Solution. Electrochim. Acta 52 (2007) 3732–3738.
[50] S. Liu, X. Qin, Preparation of a Ag–MnO_2/graphene composite for the oxygen reduction reaction in alkaline solution. RSC Adv. 5 (2015) 15627-15633.
[51] A.J. Bard, L.R. Faulkner, Electrochemical Methods, 2nd ed. John Wiley and Sons, New York, 2001.
[52] R.E. Davis, G.L. Horvath, C.W. Tobias, The solubility and diffusion coefficient of oxygen in potassium hydroxide solutions. Electrochim. Acta 12 (1967) 287-297.
[53] D.R. Lide, CRC Handbook of Chemistry and Physics, 82nd ed., CRC Press, Boca Raton, 2001.
[54] Q. Wu, J. Ruan, Z. Zhou, S. Sang, Effect of preparation routes on activity of Ag−MnOx/C as electrocatalysts for oxygen reduction reaction in alkaline media. Trans. Nonferrous Met. Soc. China 25 (2015) 510−519.

[55] F. Lima, J. Zhang, M. Shao, K. Sasaki, M. Vukmirovic, E. Ticianelli, R. Adzic, Catalytic Activity−d-band Center Correlation for the O2 Reduction Reaction on Pt in Alkaline Solutions. J. Phys. Chem. C 111 (2007) 404–410.

[56] L. Gao, Z. Li, Q. Xue, Preparation of MnO_2/graphene composite as electrode material for supercapacitors. J. Power Sources 248 (2014) 565–569.

[57] Z. Yang, X. Zhou, H. Nie, Z. Yao, S. Huang, Facile construction of manganese oxide doped carbon nanotube catalysts with high activity for oxygen reduction reaction and investigations into the origin of their activity enhancement. ACS Appl. Mater. Interfaces 3 (2011) 2601–2606.

[58] I. Roche, E. Chaînet, M. Chatenet, J. Vondrák, Durability of carbon-supported manganese oxide nanoparticles for the oxygen reduction reaction (ORR) in alkaline medium. J. Appl. Electrochem. 38 (2008) 1195–1201.

[59] B. Magnusson, T. Näykki, H. Hovind, M. Krysell, Handbook for calculation of measurement uncertainty in environmental laboratories. Nordtest, Espoo, 2003.

10.Acknowledgements

I would like to thank my supervisors Dr. Nadežda Kongi and Dr. Kaido Tammeveski for all the support, advice and guidance through the duration of doing my thesis.

Non-exclusive license to reproduce thesis and make thesis public

I, Shypunov Illia, (date of birth: 10.02.1992.),

1. herewith grant the University of Tartu a free permit (non-exclusive license) to:

1.1. reproduce, for the purpose of preservation and making available to the public, including for addition to the DSpace digital archives until expiry of the term of validity of the copyright, and

1.2. make available to the public via the university's web environment, as of 1.06.2015 until expiry of the term of validity of the copyright,

"Highly active Ag-MnO_x/C catalysts for oxygen electroreduction"

(title of thesis)

supervised by Dr. Nadežda Kongi and Dr. Kaido Tammeveski

2. I am aware of the fact that the author retains these rights.

3. This is to certify that granting the non-exclusive license does not infringe the intellectual property rights or rights arising from the Personal Data Protection Act.

Tartu 1.06.2015